NANOCATALYSTS

Platinum-based nanocages with subnanometer-thick walls and well-defined, controllable facets

Lei Zhang,[1,2] Luke T. Roling,[3] Xue Wang,[1,2] Madeline Vara,[4] Miaofang Chi,[5] Jingyue Liu,[6] Sang-Il Choi,[1] Jinho Park,[4] Jeffrey A. Herron,[3] Zhaoxiong Xie,[2] Manos Mavrikakis,[3] Younan Xia[1,4,7]*

A cost-effective catalyst should have a high dispersion of the active atoms, together with a controllable surface structure for the optimization of activity, selectivity, or both. We fabricated nanocages by depositing a few atomic layers of platinum (Pt) as conformal shells on palladium (Pd) nanocrystals with well-defined facets and then etching away the Pd templates. Density functional theory calculations suggest that the etching is initiated via a mechanism that involves the formation of vacancies through the removal of Pd atoms incorporated into the outermost layer during the deposition of Pt. With the use of Pd nanoscale cubes and octahedra as templates, we obtained Pt cubic and octahedral nanocages enclosed by {100} and {111} facets, respectively, which exhibited distinctive catalytic activities toward oxygen reduction.

One strategy to increase the utilization efficiency (UE) of platinum group metals (PGMs) is to increase the proportion of atoms exposed on the surface (the dispersion) by reducing particle size. For example, the UE of platinum (Pt) atoms can be increased from 9.5 to 26% by reducing the edge length of a Pt cube from 11.7 to 3.9 nm. Despite the extensive use of this strategy, it has been difficult to optimize the specific activity of such small nanocrystals (NCs) by engineering their surface structure through facet-controlled synthesis (*1*). Such NCs also tend to sinter (form larger particles), detach from the support, or both during operation (*2*). An alternative strategy is to use nanoframes—open nanostructures comprising multiple ridges as thin as a few nanometers (*3*–*5*). Each ridge of a nanoframe can be considered as a linear aggregate of NCs. Essentially, all the PGMs can be prepared as nanoframes by using methods that involve the selective removal of a sacrificial component: for example, the more reactive metal in alloyed NCs or the NC serving as a template for the site-selected deposition of the PGM. In a notable example, Pt_3Ni nanoframes with extraordinary mass activity of 5.7 amperes per milligram of Pt ($A\ mg^{-1}_{Pt}$) toward the oxygen reduction reaction (ORR) have been developed (*5*), but this method still faces challenges in selecting the exposed crystal facet with which to control their catalytic activity and selectivity.

A different strategy for increasing the UE of a PGM is to assemble the metal atoms into nanosheets (*6*–*8*). For such a system consisting of four atomic layers, the UE could in principle reach 50%, but the use of PGM nanosheets as catalysts encounters several drawbacks: (i) the top and bottom surfaces of a sheet must be capped by ligands; (ii) the metal atoms can only assume a hexagonal lattice, corresponding to one type of facet only; and (iii) it is challenging to deposit and expose individual nanosheets on a catalytic support. An alternative to this strategy is to deposit the PGM conformally as subnanometer-thick shells of only a few atomic layers on the surfaces of NC templates made of another metal. In addition to the electrochemical approach explored by a number of groups (*9*–*11*), we recently developed a solution-phase method for the deposition of Pt on facet-controlled palladium (Pd) NCs to generate $Pd@Pt_{nL}$ core-shell structures (where n is the number of Pt atomic layers), in which the Pt shells could be controlled at 1 to 6 atomic layers in thickness (*12*–*14*). The $Pd@Pt_{nL}$ NCs showed great improvement in terms of both mass activity and durability toward ORR relative to a commercial Pt/carbon (C) catalyst.

The interiors of these core-shell structures, however, are still occupied by another PGM (Pd, in this case), which will contribute to a large portion of the materials cost associated with such a catalyst. A logical solution is to selectively remove the Pd template after Pt deposition, generating a nanocage made of Pt only. When conducted appropriately, the facets present on the surface of a template can be well preserved during the Pt coating and Pd etching processes

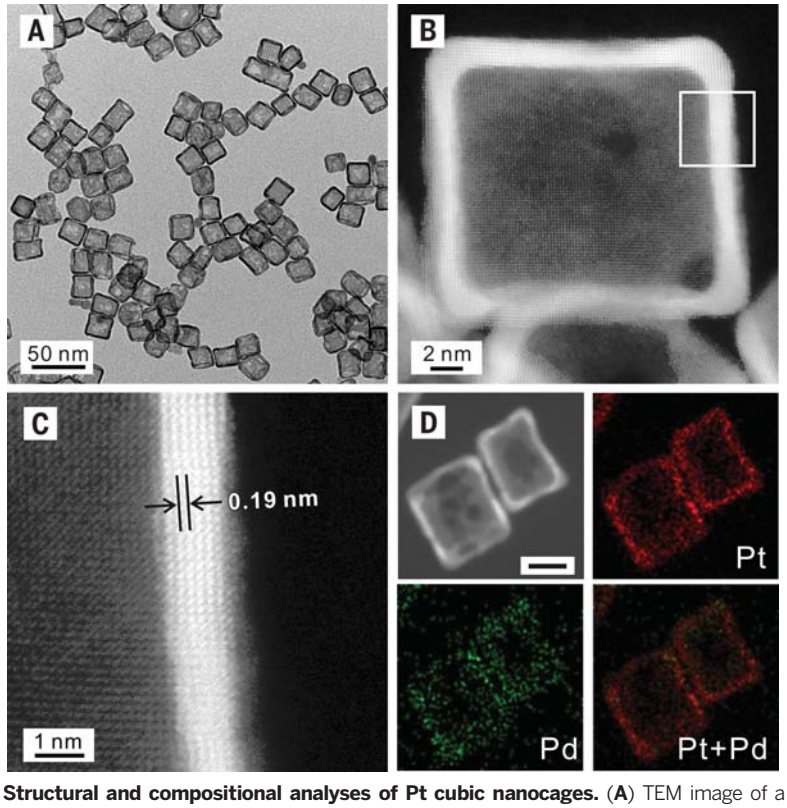

Fig. 1. Structural and compositional analyses of Pt cubic nanocages. (**A**) TEM image of a typical sample. (**B**) HAADF-STEM image of an individual nanocage. (**C**) High-resolution HAADF-STEM image taken from the region boxed in (B), showing a wall thickness of six atomic layers. (**D**) EDS elemental mapping of Pt and Pd for two nanocages. Scale bar, 10 nm.

[1]Wallace H. Coulter Department of Biomedical Engineering, Georgia Institute of Technology and Emory University, Atlanta, GA 30332, USA. [2]State Key Laboratory of Physical Chemistry of Solid Surfaces, Collaborative Innovation Center of Chemistry for Energy Materials, and Department of Chemistry, Xiamen University, Xiamen, Fujian 361005, P. R. China. [3]Department of Chemical and Biological Engineering, University of Wisconsin–Madison, Madison, WI 53706, USA. [4]School of Chemistry and Biochemistry, Georgia Institute of Technology, Atlanta, GA 30332, USA. [5]Center for Nanophase Materials Sciences, Oak Ridge National Laboratory, Oak Ridge, TN 37831, USA. [6]Department of Physics, Arizona State University, Tempe, AZ 85287, USA. [7]School of Chemical and Biomolecular Engineering, Georgia Institute of Technology, Atlanta, GA 30332, USA.
*Corresponding author. E-mail: younan.xia@bme.gatech.edu

so as to engineer the activity and/or selectivity of the catalyst. We demonstrate this concept by coating the surfaces of Pd nanoscale cubes and octahedra with four atomic layers of Pt, followed by selective removal of the Pd templates. Density functional theory (DFT) calculations suggest that the etching is initiated via a mechanism that involves the formation of surface vacancies by etching away Pd atoms incorporated into the Pt shells from intermixing and/or co-reduction (*15*). We could obtain Pt nanocages with walls as thin as three atomic layers (0.7 nm thick), with their surfaces terminated in {100} or {111} facets. The nanocages show distinctive specific activities toward ORR depending on the exposed facet, whereas the activity and durability are both enhanced relative to a commercial Pt/C catalyst.

We first synthesized Pd cubes with an average edge length of 18.2 nm (fig. S1, A and B) (*16*, *17*). Four atomic layers of Pt were then deposited on the surface of each Pd cube as a conformal shell (fig. S1C) by introducing a Pt(IV) precursor at 200°C (*12*). The use of a slow injection rate and a relatively high temperature resulted in the formation of core-shell cubes with atomically flat surfaces (*18*). When subjected to etching, the Pd templates could be selectively removed to leave behind Pt cubic nanocages with ultrathin walls covered by {100} facets.

A transmission electron microscopy (TEM) image of Pt cubic nanocages derived from Pd@Pt_{4L} cubes by using a standard procedure is shown in Fig. 1A (*17*). The nanocages had an average edge length of 20.2 nm (fig. S1D), together with small holes on the surfaces. The high-angle annular dark-field scanning TEM (HAADF-STEM) image (Fig. 1B) taken from one of the nanocages revealed a periodic lattice extending across the entire surface, suggesting that the single-crystal structure of the Pd template was transferred to the Pt shell. The uniform contrast across the side face indicates that essentially all the Pd atoms in the core had been removed, except for those alloyed with Pt atoms in the walls. The atomic-resolution HAADF-STEM image (Fig. 1C) recorded from the region boxed in Fig. 1B indicates a wall thickness of ~1 nm, corresponding to six atomic layers along the [100] direction. The lattice spacing of 0.19 nm can be assigned to the (200) planes of face-centered cubic (fcc) Pt.

Although only four atomic layers of Pt were initially deposited on the surface of each Pd template, the wall thickness increased to six atomic

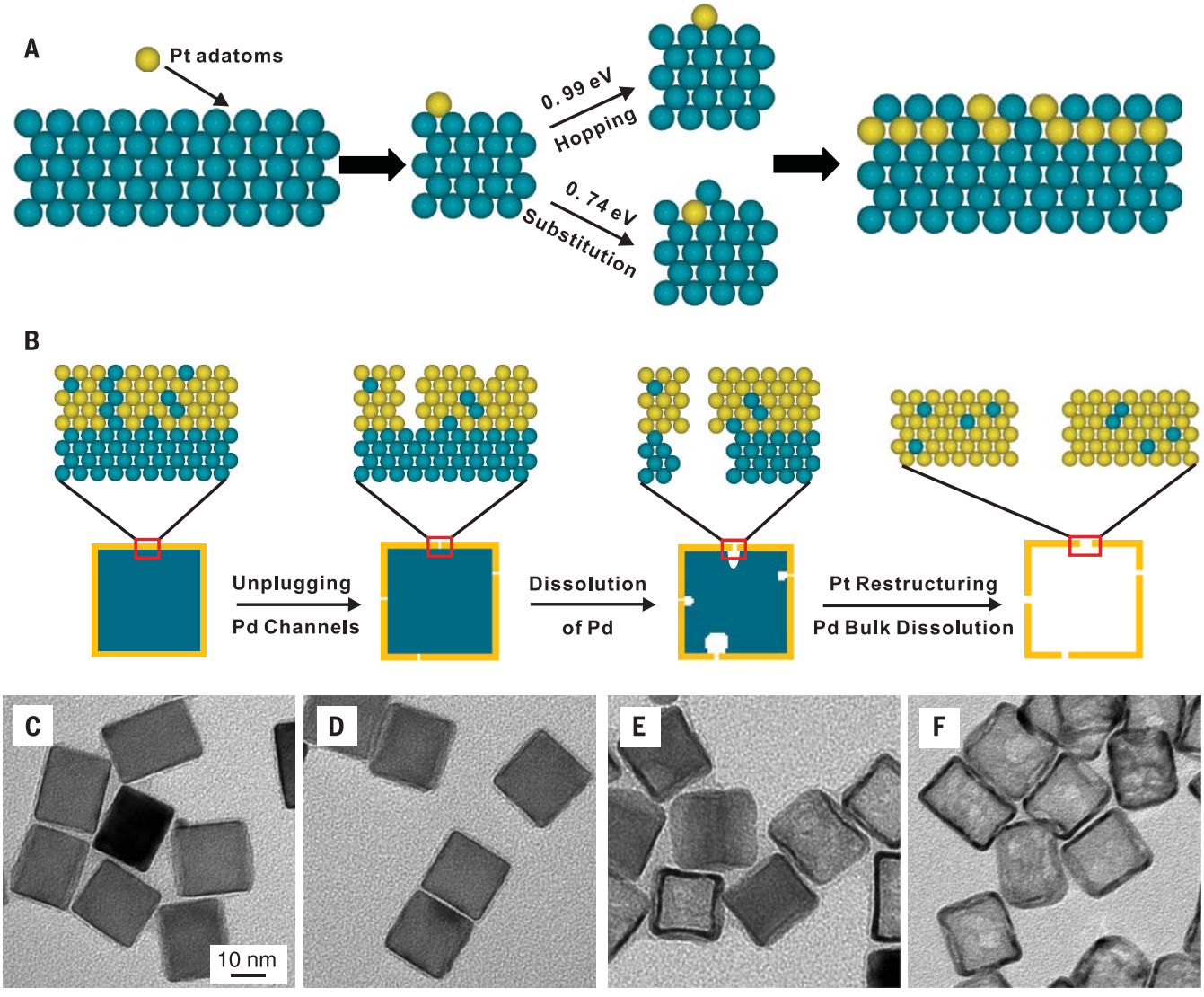

Fig. 2. Mechanistic details involved in the deposition and etching processes, and TEM images of the products obtained after etching for different periods of time. (**A**) Pt atoms deposited on the Pd surface may diffuse ("hop") across the surface or substitute into the surface (DFT-calculated activation barriers are shown), leading to a mixed outer-layer composition. (**B**) Schematic of the major steps involved in the continuous dissolution of Pd atoms from a Pd@Pt_{4L} cube to generate a Pt cubic nanocage. (**C** to **F**) TEM images of Pd@Pt_{4L} cubes after Pd etching for (C) 0, (D) 10, (E) 30, and (F) 180 min. Scale bar, 10 nm, applies to (C) to (F).

layers because of the following factors: the interdiffusion and alloying between Pt and Pd, and thus a small amount of Pd remains in the walls; the inclusion of small holes in the side faces; and the migration of atoms from side faces to ridges, making the walls appear thicker under TEM. Elemental mapping based on energy-dispersive x-ray spectroscopy (EDS) confirmed that the nanocages were composed of a Pt-Pd alloy (Fig. 1D). Inductively coupled plasma mass spectrometry (ICP-MS) analysis gave Pt mass percentages of 93.6 and 33.9% for the nanocages and core-shell cubes, respectively.

We hypothesize that the etching is initiated by oxidizing the Pd atoms in the outmost layer of the Pt shell to generate vacancies, followed by diffusion of Pd atoms from underlying layers to generate more vacancies (*15*). This process is similar to the mechanism proposed by Heggen *et al.* for the electrochemical dealloying of Co-Pt core-shell nanoparticles (*19*), but in our case, we were able to completely remove the Pd cores because of the involvement of ultrathin Pt shells and the persistence of pores in the shells. Previous work by Erlebacher *et al.* emphasized the role of mobile, low-coordinated metal atoms in a dealloying process because movement and clustering of these species continually exposed less noble atoms for dissolution (*20*). These observations may explain the restructuring of our atomic-width vacancies to larger pores, allowing more bulk-like dissolution of Pd from the core. In contrast, our system consists of ultrathin, smooth Pt surfaces with a relatively low Pd concentration. The amount of low-coordinated Pt should therefore be low, and surface restructuring is limited to areas near the atom-wide channels formed in the initial stage. We performed DFT calculations to evaluate the diffusion barrier of a Pd atom though the Pt shell using a fully relaxed Pt(100) membrane of four atomic layers as a model system (*17*). We examined a number of processes (such as one-to-one atom exchange, as well as three-body and four-body rotations), and concluded that (i) diffusion of Pd and Pt atoms through Pt, at 100°C, must be vacancy-mediated, and (ii) the lowest diffusion barrier is for Pd through Pt (0.88 eV). Previous experimental studies of Pd-Pt interdiffusion also found that Pd had a higher diffusion rate in Pt than in Pd (*21*).

Because diffusion must occur at vacancies in our model, we also considered the mechanism by which the vacancies arise. We believe that Pt-Pd intermixing occurs during the deposition of Pt (Fig. 2A), rather than after the formation of perfect Pt overlayers. The deposition was conducted at a relatively high temperature so as to give Pt atoms an opportunity to spread across the Pd surface and thus grow in a layer-by-layer fashion (*18*). Using DFT, we obtained an energy barrier of 0.99 eV for the diffusion of Pt adatoms across a Pd(100) surface (a "hopping" mechanism). However, a Pt adatom can instead substitute into the Pd surface, pushing the Pd atom to a nearby hollow surface site with a barrier of just 0.74 eV (a "substitution" mechanism); this process is exothermic by 0.38 eV. As a consequence of these two mechanisms, some Pd atoms will be incorporated into the Pt shell as each Pt overlayer is formed. The activation energy barrier for Pt substitution increases as the Pt coverage increases, so not all of the Pd atoms will be substituted by Pt atoms when each additional layer of Pt is deposited. Alternatively, Pd atoms can be incorporated into the Pt shell through a co-reduction mechanism. Because the synthesis was conducted in air at 200°C, a trace amount of Pd atoms on the templates could be oxidized and released into the reaction solution as Pd(II) ions before the introduction of Pt(IV) precursor. Subsequently, the Pd(II) and Pt(IV) ions would be co-reduced and deposited onto the templates to generate Pt shells doped with Pd atoms. Before the introduction of Pt(IV) precursor, however, the concentration of Pd(II) ions in the reaction solution was too low to be detected with ICP-MS.

A plausible mechanism involved in the formation of a Pt cubic nanocage from a Pd@Pt_{nL} cube is illustrated in Fig. 2B. During Pt deposition, some Pd atoms are incorporated into the Pt overlayers through intermixing and/or co-reduction. Upon contact with the etchant, the Pd atoms in the outermost layer are oxidized so as to generate surface vacancies. The underlying Pd atoms then diffuse to these vacancies and are continuously etched away, leaving behind atom-wide channels. In the early stage of etching, the diffusion of Pd through these channels leads to a Kirkendall effect because Pd diffuses outward faster than Pt diffuses inward, creating a void in the Pd template. Over time, the channels will grow in size (and also reconstruct) to allow direct corrosion of Pd from the core. TEM images of the initial Pd@Pt_{4L} cubes and the same batch of sample after etching with a standard procedure for 10 min are shown in Fig. 2, C and D, respectively. There were essentially no changes to the shape, morphology, or structure of the core-shell cubes. According to ICP-MS analysis, the Pd mass percentage of this sample was 63.5%, which only dropped slightly from the initial value of 66.1%. The data suggest that the initial etching only involved "unplugging" of the existing Pd atoms on the outermost layer of the Pt shell. In a control experiment, we noticed that the Pd etching could be initiated at a much faster rate and at a lower temperature by cotitrating Pd(II) and Pt(IV) precursors at a molar ratio of 1:99 during the deposition of Pt (fig. S2). Our results also indicate that the etching rate could be manipulated by varying the molar ratio of Pd(II) to Pt(IV) precursors.

Once initiated, the surface layers begin to undergo reconstruction facilitated by the high etching temperature, enlarging the channels to 1 to 3 nm wide for direct corrosion of Pd. As shown in Fig. 2E, most of the Pd@Pt_{4L} cubes had

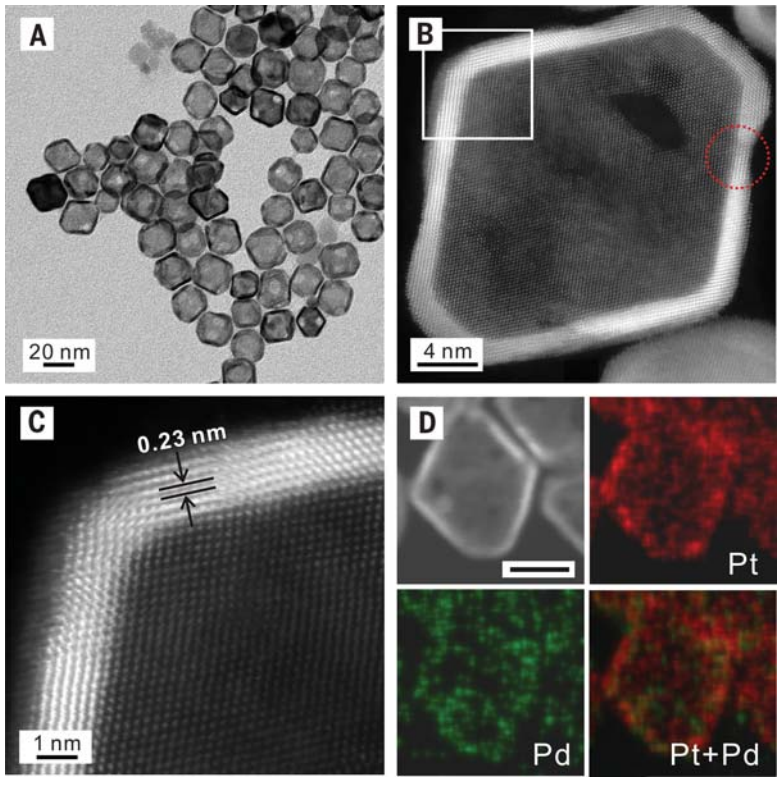

Fig. 3. Structural and compositional analyses of Pt octahedral nanocages. (**A**) TEM image of a typical sample. (**B**) HAADF-STEM image of an individual nanocage. The red circle marks a hole responsible for the dissolution of Pd from the core. (**C**) High-resolution HAADF-STEM image taken from the region boxed in (B), showing a wall thickness of seven atomic layers. (**D**) EDS mapping of Pt and Pd. Scale bar, 10 nm.

evolved into hollow structures after etching for 30 min. At the same time, the Pd mass percentage quickly dropped to 21.9%. Further etching led to Pt cubic nanocages characterized by a completely hollow interior and porous walls. Shown in Fig. 2F is a TEM image of the product obtained after etching for 3 hours and the Pd mass percentage had dropped to 6.4%. At this point, the removal of Pd was essentially completed because the Pd mass percentage did not show any change when the etching time was prolonged to 4 hours. We noted that Pt nanocages derived from $Pd@Pt_{2\text{-}3L}$ cubes (fig. S3A) tended to collapse when the standard procedure was used for etching but could be largely preserved under milder etching conditions (fig. S3, B to D).

The arrangement of atoms on the surface can affect both catalytic activity and selectivity; for example, Pt(111) is more active toward ORR than is Pt(100) (*22*). Thus, we extended Pt deposition and Pd etching procedures to the preparation of Pt octahedral nanocages enclosed by {111} facets (Fig. 3A). We prepared $Pd@Pt_{4\text{-}5L}$ octahedra from Pd octahedra of 19.4 nm in edge length (fig. S4) (*16*, *20*) and then etched away the Pd templates using more etchant relative to the standard procedure. The HAADF-STEM image in Fig. 3B shows a lattice spacing of 0.23 nm that can be assigned to the {111} planes of fcc Pt. The atomic-resolution HAADF-STEM image in Fig. 3C indicates the presence of seven atomic layers of Pt in the shell. The inclusion of Pd in the walls was confirmed with EDS (Fig. 3D). According to our ICP-MS analysis, the Pd mass percentage of the octahedral nanocages was only 9.1%, indicating the completion of template removal. By switching to $Pd@Pt_{2\text{-}3L}$ octahedra, we were able to obtain Pt octahedral nanocages with a wall thickness of only three atomic layers [or 0.7 nm along the [111] direction (fig. S5)] using a standard procedure.

We used ORR as a model reaction to demonstrate the ability to engineer the catalytic activity of such Pt nanocages by manipulating the type of facet exposed on the surface. We benchmarked their catalytic performance against a commercial Pt/C catalyst (table S1 and fig. S6). We used cyclic voltammetry (CV) to measure the electrochemically active surface area (ECSA) of each catalyst. The specific ECSAs of cubic and octahedral nanocages were measured as 46.8 and 38.2 square meters per gram of Pt ($m^2\ g^{-1}_{Pt}$), respectively, which are comparable with the value of 44.2 $m^2\ g^{-1}_{Pt}$ reported for Pt_3Ni nanoframes (*5*). Although the surfaces of the nanocages are covered by small holes (~20% of the total surface area), their ECSAs were still similar to those of the corresponding $Pd@Pt_{nL}$ NCs—39.7 and 38.0 $m^2\ g^{-1}_{Pt}$, respectively—for the cubic and octahedral systems (*12*, *13*) because of the contribution from the inner surface. The specific ECSAs of the nanocages were also on par with that of the Pt/C catalyst (56.8 $m^2\ g^{-1}_{Pt}$), even though their sizes differ more than sevenfold (20 versus 2.8 nm).

We then evaluated the electrocatalytic performance of the different catalysts toward ORR (fig. S6, B to D). As displayed in Fig. 4A, the octahedral nanocages had mass activity of 0.75 A mg^{-1}_{Pt} at 0.9 volts versus reversible hydrogen electrode (V_{RHE}), which was five times greater than the Pt/C reference (0.14 A mg^{-1}_{Pt}). The results demonstrate that the transformation from $Pd@Pt_{nL}$ NCs into Pt nanocages could greatly improve the catalytic performance toward ORR in terms of Pt mass and materials cost. This catalytic system, however, needs to be optimized before it can compete with the more active (but more complex) system based on Pt-Ni alloys (*5*, *23*–*28*). As shown in Fig. 4B, the octahedral nanocages exhibited the highest specific activity, with a value of 1.98 mA cm^{-2} at 0.9 V_{RHE}, which was almost eight times greater than that of the Pt/C (0.25 mA cm^{-2}). The almost twofold difference in specific activity between the octahedral and cubic nanocages clearly demonstrates the feasibility to control the catalytic activity of such nanocages through facet engineering. We used DFT to analyze the ORR-specific activities of the nanocages by calculating the energetics of OH

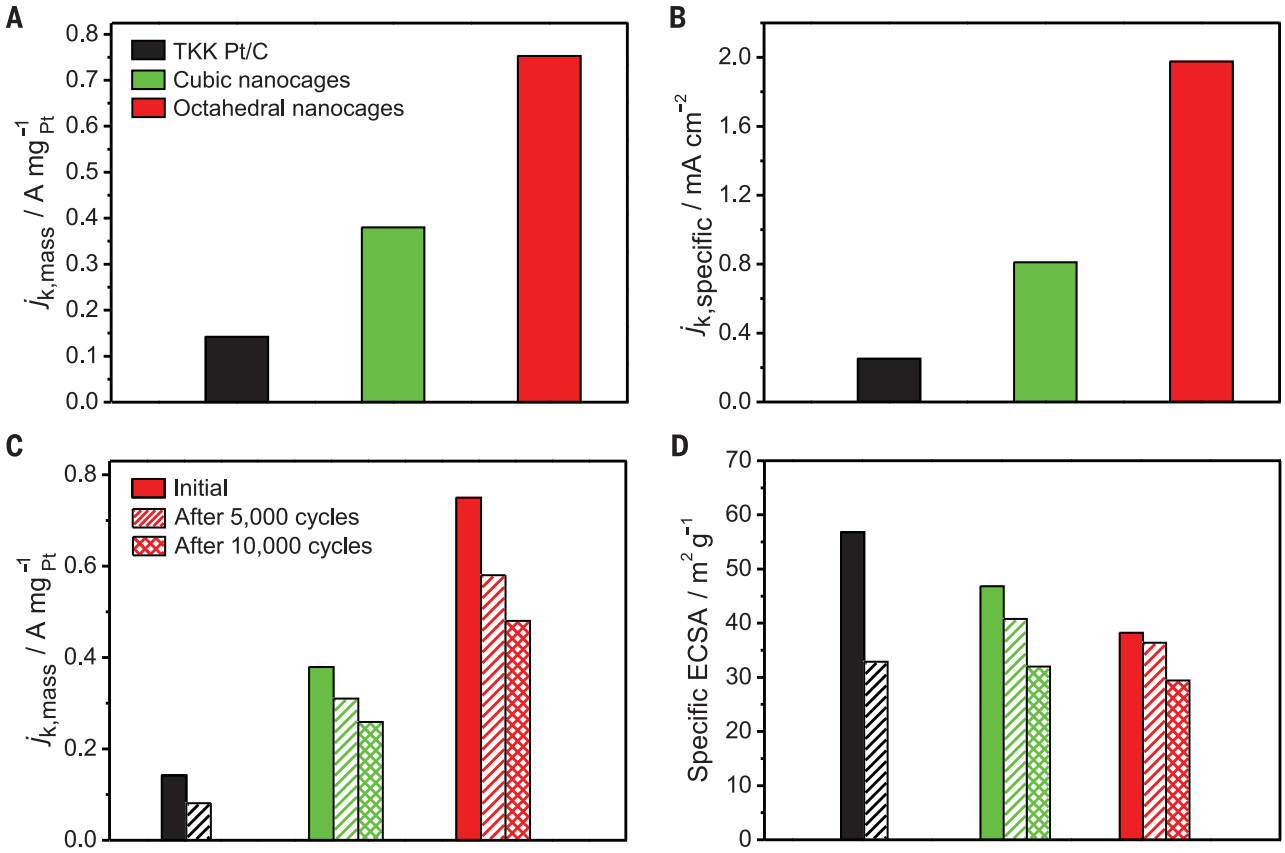

Fig. 4. Electrocatalytic properties of Pt nanocages relative to a commercial Pt/C catalyst. (**A**) Mass and (**B**) specific activities of the catalysts at 0.9 V_{RHE}. (**C**) Mass activities (at 0.9 V_{RHE}) and (**D**) specific ECSAs of the catalysts before and after accelerated durability test. The color scheme applies to all panels.

removal, which has been shown to be the rate-determining step on similar surfaces (*12*–*14*, *17*). Relative to their core-shell precursors, the nanocage models showed substantially enhanced activity, which is attributed to the shortening of Pt-Pt interatomic distances (table S2).

We evaluated the long-term stability of the catalysts through an accelerated durability test (Fig. 4, C and D). The Pt octahedral nanocages showed the best performance, with the ORR mass activity only reduced by 36% after 10,000 cycles, still showing 3.4-fold enhancement relative to the pristine Pt/C. The ECSAs of the cubic and octahedral nanocages only dropped by 13 and 6% after 5000 cycles and by 32 and 23% after 10,000 cycles, respectively. During the durability test, the holes in the walls of the nanocages were slightly enlarged (fig. S7). These results demonstrate that the excellent durability associated with the core-shell catalysts was not affected by the selective removal of Pd cores.

REFERENCES AND NOTES

1. J. Chen, B. Lim, E. P. Lee, Y. Xia, *Nano Today* **4**, 81–95 (2009).
2. F. A. de Bruijn, V. A. T. Dam, G. J. M. Janssen, *Fuel Cells (Weinh.)* **8**, 3–22 (2008).
3. X. Lu *et al.*, *Nano Lett.* **7**, 1764–1769 (2007).
4. S. Xie *et al.*, *Angew. Chem. Int. Ed. Engl.* **51**, 10266–10270 (2012).
5. C. Chen *et al.*, *Science* **343**, 1339–1343 (2014).
6. A. Funatsu *et al.*, *Chem. Commun. (Camb.)* **50**, 8503–8506 (2014).
7. H. Li *et al.*, *Angew. Chem. Int. Ed. Engl.* **52**, 8368–8372 (2013).
8. H. Duan *et al.*, *Nat. Commun.* **5**, 3093 (2014).
9. R. R. Adzic *et al.*, *Top. Catal.* **46**, 249–262 (2007).
10. K. Sasaki *et al.*, *Nat. Commun.* **3**, 1115 (2012).
11. M. Shao *et al.*, *Chem. Commun. (Camb.)* **49**, 9030–9032 (2013).
12. S. Xie *et al.*, *Nano Lett.* **14**, 3570–3576 (2014).
13. J. Park *et al.*, *ACS Nano* **9**, 2635–2647 (2015).
14. X. Wang *et al.*, *Nat. Commun.* **6**, 7594 (2015).
15. Y. Yin *et al.*, *Science* **304**, 711–714 (2004).
16. M. Jin *et al.*, *Nano Res.* **4**, 83–91 (2011).
17. Materials and methods are available as supplementary materials on *Science* Online.
18. X. Xia *et al.*, *Proc. Natl. Acad. Sci. U.S.A.* **110**, 6669–6673 (2013).
19. M. Heggen, M. Oezaslan, L. Houben, P. Strasser, *J. Phys. Chem. C* **116**, 19073–19083 (2012).
20. J. Erlebacher, M. J. Aziz, A. Karma, N. Dimitrov, K. Sieradzki, *Nature* **410**, 450–453 (2001).
21. V. A. Baheti, R. Ravi, A. Paul, *J. Mater. Sci. Mater. Electron.* **24**, 2833–2838 (2013).
22. N. M. Markovic, P. N. Ross, *Surf. Sci. Rep.* **45**, 117–229 (2002).
23. J. Zhang, H. Yang, J. Fang, S. Zou, *Nano Lett.* **10**, 638–644 (2010).
24. J. Wu, A. Gross, H. Yang, *Nano Lett.* **11**, 798–802 (2011).
25. S.-I. Choi *et al.*, *Nano Lett.* **13**, 3420–3425 (2013).
26. C. Cui, L. Gan, M. Heggen, S. Rudi, P. Strasser, *Nat. Mater.* **12**, 765–771 (2013).
27. L. Gan *et al.*, *Science* **346**, 1502–1506 (2014).
28. B. Han *et al.*, *Energy Environ. Sci.* **8**, 258–266 (2015).

ACKNOWLEDGMENTS

The syntheses were supported by start-up funds from the Georgia Institute of Technology (to Y.X.). As jointly supervised PhD students from Xiamen University, L.Z. and X.W. were also partially supported by fellowships from the China Scholarship Council. The theoretical modeling work at University of Wisconsin–Madison was supported by the U.S. Department of Energy (DOE)–Basic Energy Sciences (BES), Office of Chemical Sciences, grant DE-FG02-05ER15731. Calculations were performed at supercomputing centers located at the Environmental Molecular Sciences Laboratory, which is sponsored by the DOE Office of Biological and Environmental Research at the Pacific Northwest National Laboratory; Center for Nanoscale Materials at Argonne National Laboratory, supported by DOE contract DE-AC02-06CH11357; and National Energy Research Scientific Computing Center, supported by DOE contract DE-AC02-05CH11231. Part of the electron microscopy work was performed through a user project supported by the Oak Ridge National Laboratory's Center for Nanophase Materials Sciences, which is a DOE Office of Science User Facility. J.L. gratefully acknowledges the support by Arizona State University and the use of facilities in the John M. Cowley Center for High Resolution Electron Microscopy at Arizona State University. Data described can be found in the main figures and supplementary materials. The authors declare no conflict of interests.

SUPPLEMENTARY MATERIALS

www.sciencemag.org/content/349/6246/412/suppl/DC1
Materials and Methods
Figs. S1 to S8
Tables S1 to S3
References (*29*–*37*)

8 March 2015; accepted 15 June 2015
10.1126/science.aab0801

EVOLUTION

A four-legged snake from the Early Cretaceous of Gondwana

David M. Martill,[1] Helmut Tischlinger,[2] Nicholas R. Longrich[3]

Snakes are a remarkably diverse and successful group today, but their evolutionary origins are obscure. The discovery of snakes with two legs has shed light on the transition from lizards to snakes, but no snake has been described with four limbs, and the ecology of early snakes is poorly known. We describe a four-limbed snake from the Early Cretaceous (Aptian) Crato Formation of Brazil. The snake has a serpentiform body plan with an elongate trunk, short tail, and large ventral scales suggesting characteristic serpentine locomotion, yet retains small prehensile limbs. Skull and body proportions as well as reduced neural spines indicate fossorial adaptation, suggesting that snakes evolved from burrowing rather than marine ancestors. Hooked teeth, an intramandibular joint, a flexible spine capable of constricting prey, and the presence of vertebrate remains in the guts indicate that this species preyed on vertebrates and that snakes made the transition to carnivory early in their history. The structure of the limbs suggests that they were adapted for grasping, either to seize prey or as claspers during mating. Together with a diverse fauna of basal snakes from the Cretaceous of South America, Africa, and India, this snake suggests that crown Serpentes originated in Gondwana.

Snakes are among the most diverse groups of tetrapods, with >3000 extant species exploiting a remarkable range of niches (*1*). Snakes inhabit deserts and rainforests, mountains and oceans; and despite lacking limbs, employ an extraordinary range of locomotor styles, including crawling, burrowing, climbing, swimming, and even gliding (*1*). All snakes are predators, but they consume a wide range of prey, from insects to large mammals (*1*). This diversity is made possible by a specialized body plan, including an elongate body with reduced limbs, a flexible skull and ribs to swallow large prey (*2*), and a specialized forked tongue and vomeronasal organ to detect chemical gradients (*1*). The origins of this body plan remain unclear, however (*1*). One scenario holds that it originated in a marine environment, whereas others argue that it results from adaptation for a fossorial lifestyle. New fossils (*2*–*4*), including snakes with hindlimbs (*5*, *6*), have shed light on the lizard-to-snake transition, but no snake has been reported with four limbs. The ecology of early snakes is also uncertain. Although alethinophidians are primarily carnivorous (*1*), Typhlopidae and Anomalepididae, which are basal with respect to Alethinophidia (*7*–*9*), are insectivorous (*1*). This suggests that early snakes were insectivores, although adaptations for carnivory in stem snakes (*2*) suggest that carnivory may be primitive (*2*, *5*).

Here we report a fossil snake from the Early Cretaceous of Gondwana, which sheds light on these issues. *Tetrapodophis amplectus* gen. et sp. nov. (holotype BMMS BK 2-2) is distinguished from all other snakes by the following combination of characters: 160 precaudal and 112 caudal vertebrae, short neural spines, four limbs, metapodials short, penultimate phalanges hyperelongate and curved, phalangeal formula 2?-3-3-3-3? (manus) 2-3-3-3-3 (pes).

The fossil (Fig. 1) comes from the Nova Olinda Member of the Early Cretaceous (Aptian) Crato Formation, Ceará, Brazil (*10*). The specimen is preserved on laminated limestone as part and counterpart. The matrix is typical of the Nova Olinda Member in being composed of fine-grained laminated micrite with elongated pellets on the surface of the slab representing coprolites of the fish *Dastilbe*. As is typical of Crato vertebrates, the skeleton is articulated and the bones are a translucent orange-brown color; soft tissues are also preserved.

The snake affinities of *Tetrapodophis* are demonstrated by derived features of the skull, axial

[1]School of Earth and Environmental Sciences, University of Portsmouth, Portsmouth PO1 3QL, UK. [2]Tannenweg 16, 85134 Stammham, Germany. [3]Department of Biology and Biochemistry and Milner Centre for Evolution, University of Bath, Claverton Down, Bath BA2 7AY, UK.

Science
AAAS

Platinum-based nanocages with subnanometer-thick walls and well-defined, controllable facets

Lei Zhang *et al.*

Science **349**, 412 (2015);
DOI: 10.1126/science.aab0801

Science (print ISSN 0036-8075; online ISSN 1095-9203) is published weekly, except the last week in December, by the American Association for the Advancement of Science, 1200 New York Avenue NW, Washington, DC 20005.